Supporting information for: High redox performance of Y0.5Ba0.5CoO3-δ for thermochemical oxygen production and separation

M. Ezbiri[a], A. Reinhart[a], B. Huber[a], K. M. Allen[b], A. Steinfeld,[a] B. Bulfin,[a] R. Michalsky[a],

[a] Department of Mechanical and Process Engineering, ETH Zürich, 8092 Zürich, Switzerland
[b] Solar Technology Laboratory, Paul Scherrer Institute, 5232 Villigen, Switzerland

Overview Supporting Information

1. **Computational details**
    a. Structure optimizations
    b. Free energy computations
    c. Scaling relations
2. **Supporting data**
    a. XRD scans
    b. SEM data
    c. BET
    d. TGA data
    e. Molar heat capacity
    f. PBR data
    g. Energy balance equations
    h. Thermochemical equilibrium analysis
    i. Electronic structure calculations
3. **References**

1. Computational details

a. Structure optimizations

Both, ASE and GPAW are open-source codes available from the Department of Physics at the Technical University of Denmark and are available at https://wiki.fysik.dtu.dk/ase/ and https://wiki.fysik.dtu.dk/gpaw/.

We note that the lattice constants computed by DFT compare well, within the uncertainty of DFT calculations, with the experimental values of cubic perovskites with similar composition.[1, 2] For example, the DFT-computed 3.920 Å (YBCO) is 1.6% smaller than the experimental value 3.98 Å ($Ba_{0.5}Sr_{0.5}Co_{0.8}Fe_{0.2}O_3$)[3], while 3.976 Å (LBCO) is 2.9% larger than 3.862 Å (LBCO)[4], respectively.

b. Free energy computations

Free energies of the chemical species i (G_i) were calculated via:[1]

$$G_i(T,P) = N_i \mu_i(T,P) = E_i + U_{ZPE,i} - TS_i(T,P) \tag{1}$$

where T and P are the absolute temperature (298.15 K) and pressure (1.013 bar), N_i is the number of atoms, μ_i is the chemical potential, E_i is the total electronic energy determined from DFT-based structure optimization, $U_{\mathrm{ZPE},i}$ is the zero-point vibrational energy, and S_i is the entropy. Gases are assumed to be ideal, while liberated lattice oxygen is treated using the harmonic approximation where all degrees of freedom are treated as frustrated harmonic vibrations and pressure-volume contributions are neglected. Thermodynamic properties were calculated from vibrational frequencies and standard statistical mechanical equations evaluated through ASE. Free energy corrections of the solids are neglected.[5]

Analogously, the enthalpy of forming oxygen vacancies (ΔH_{v}[O]) at the surface is defined as:

$$\Delta H_{\mathrm{v}}[\mathrm{O}] = \Delta G_{\mathrm{v}}[\mathrm{O}] + \mathrm{T}\Delta S_{\mathrm{v}}[\mathrm{O}] \tag{2}$$

where ΔS_{v}[O] is the entropy of forming oxygen vacancies.

Throughout this work, free energies and enthalpies are given relative to the chemical potential of stable H_2O and H_2 in the gas phase, that is, E_O^r is given with:[1]

$$E_O^{\mathrm{r}} = E[\mathrm{H_2O}] - E[\mathrm{H_2}] \tag{3}$$

where $E[\mathrm{H_2O}]$ and $E[\mathrm{H_2}]$ are the total electronic energy of reference H_2O and H_2 molecules in the gas phase.

c. Scaling relations

Eq. (5) in the paper is based on data for TiO_2 in rutile crystal structure, Ti_2O_3, Cu_2O, ZnO in wurtzite crystal structure, MoO_3, Ag_2O, cubic $Ba_{0.5}Sr_{0.5}Co_{0.5}Fe_{0.5}$, and cubic $La_{0.5}Sr_{0.5}Co_{0.5}Fe_{0.5}$. Data for cubic ZrO_2, cubic $Y_2Zr_6O_{15}$, yttria-stabilized ZrO_2, CeO_2, and $La_{0.67}Sr_{0.33}MnO_3$ was disregarded due to a large deviation of the oxygen nonstoichiometry (δ) between the thermochemical data for the bulk metal oxides and the DFT-data for the oxygen vacancy formation energetics at the metal oxide surface.[6] That is, differences of factor 16-32 for the nonstoichiometry of ZrO_2 ($\delta = 2$ for the ZrO_2/Zr bulk couple vs. $\delta = 0.0625$ for the $Zr_{16}O_{32}/Zr_{16}O_{31}$ surface model couple), $Y_2Zr_6O_{15}$ ($\delta = 2$ for the ZrO_2/Zr bulk couple vs. $\delta = 0.0625$ for the $Y_4Zr_{12}O_{30}/Y_4Zr_{12}O_{29}$ surface model couple), CeO_2 ($\delta = 1$ for the CeO_2/Ce_2O_3 bulk couple vs. $\delta = 0.0625$ for the $Ce_{16}O_{32}/Ce_{16}O_{31}$ surface model couple), and of factor 3, which is relatively high when compared to the other computed perovskite models, for $La_{0.67}Sr_{0.33}MnO_3$ ($\delta = 1$ for the Mn_2O_3/MnO bulk couple vs. $\delta = 0.33$ for the $La_2SrMn_3O_9/La_2SrMn_3O_8$ surface model couple).

Calculations of $\Delta\bar{g}^{o*}_{O_2}$ at 773 K, respresentative for reduction, and $-\Delta\bar{g}^{o*}_{O_2}$ at 563 K, representative for oxidation, for metal oxides where the underpinning thermochemical data is not available, namely the perovskites evaluated in this work, were based on the scaling of these two bulk quantities with $\Delta\bar{h}^{o*}_{O_2}$ at 298 K and 1 bar across 38 solid metal oxide and six metal/metal oxide pairs. Thermodynamic properties obtained through scaling relations are defined per mole of monoatomic oxygen. The data for the derived linear scaling relations ($R^2 > 0.83$) are shown with Table S2, where a and b represent the following factors in Eq. (6):

$$\Delta\bar{g}^{o*}_{O_2} = a\cdot\frac{\text{kJ mol}^{-1}_{O_2}}{\text{kJ mol}^{-1}_{O_2}}\Delta\bar{h}^{o*}_{O_2} + b\ \text{kJ mol}^{-1}_{O_2} \qquad (4)$$

Table S2. DFT-derived linear scaling factors a and b, based on the scaling of $\Delta\bar{g}^{o*}_{O}$ with at 298 K and 1 bar across 27 solid metal oxide and six metal/metal oxide pairs.

	T (K)	pO_2 (bar O_2)	a	b
$\Delta\bar{g}^{o*}_{O_2}$	773	0.2	0.934	-114.366
$-\Delta\bar{g}^{o*}_{O_2}$	563	0.01	0.942	-90.342

The data for the derived linear scaling relations is given with Table S4, S5 and S6, while Table S7, S8 and S9 give the free energies of the oxide oxidation and oxide reduction that were computed with Eq. (6) ($R^2 > 0.92$) for the three studied perovskite compositions.

2. Supporting data

a. XRD scans

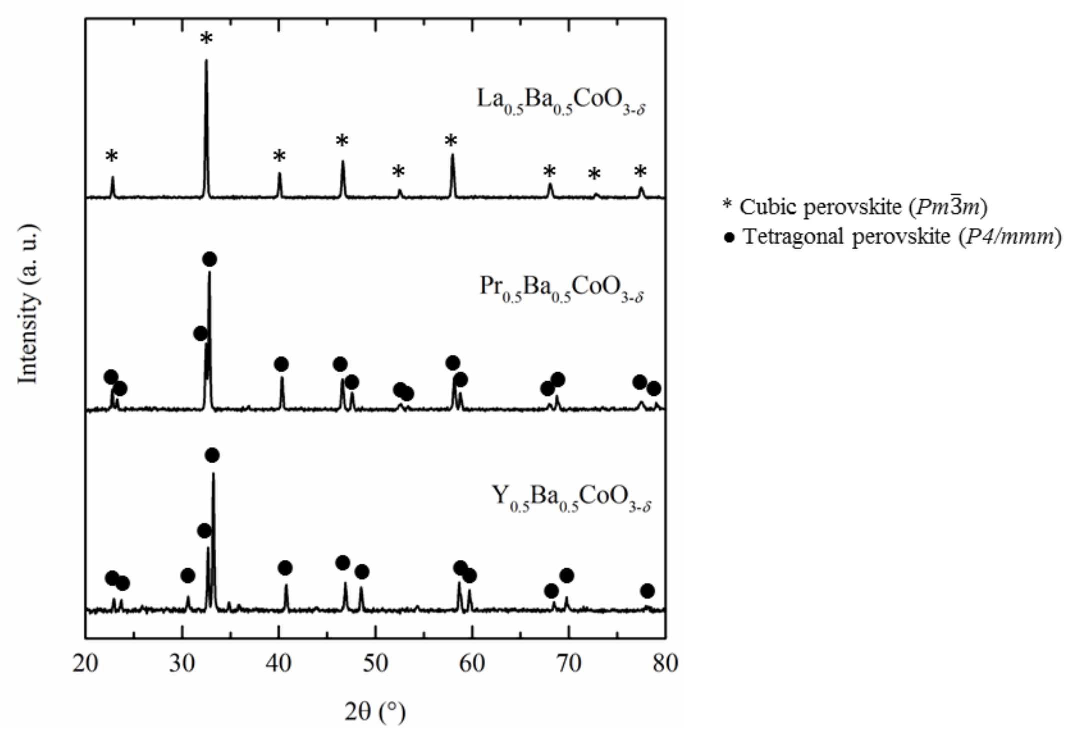

Figure S1: XRD spectra between 20 and 80° of LBCO, PBCO and YBCO pellets. XRD peak labels for LBCO obtained from Nakajima *et al.*[7], for PBCO obtained from Seikh *et al.*[8] and for YBCO obtained from Vogt *et al.*[9]

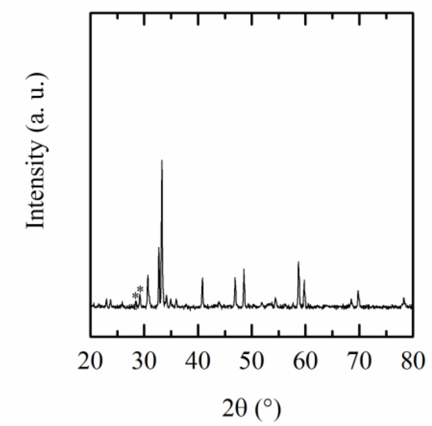

Figure S2: XRD spectrum between 20 and 80° of YBCO granules. Symbols (*) indicate additional peaks compared to the one of the YBCO pellet (*cf*. Fig. S1).

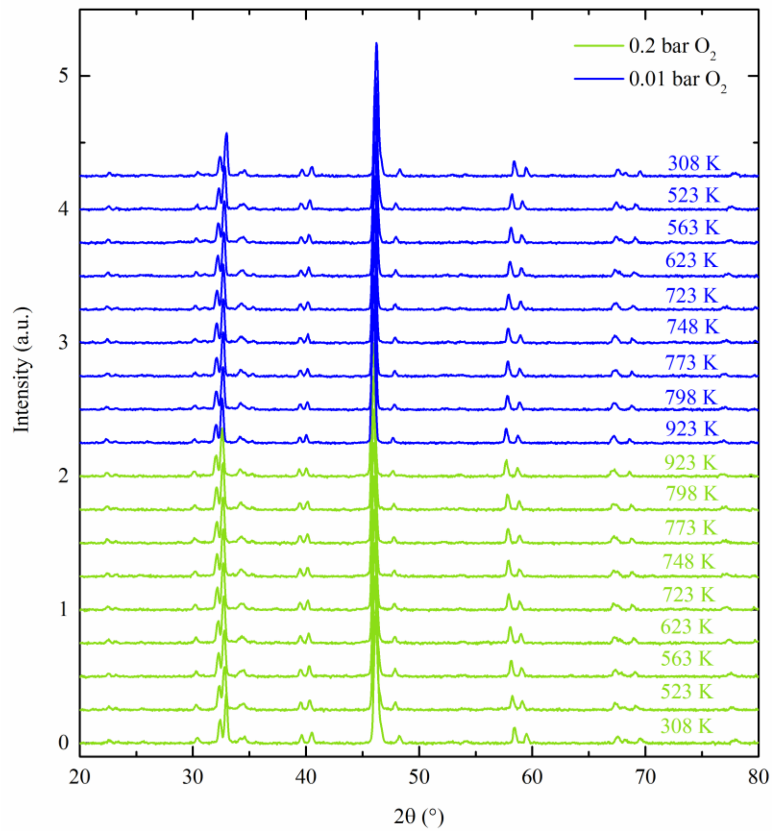

Figure S3: HT-XRD scans between 20 and 80° of YBCO between 308 and 923 K, in 0.2 bar O_2 during heating (green scans) and 0.01 bar O_2 during cooling (blue scans).

b. SEM data

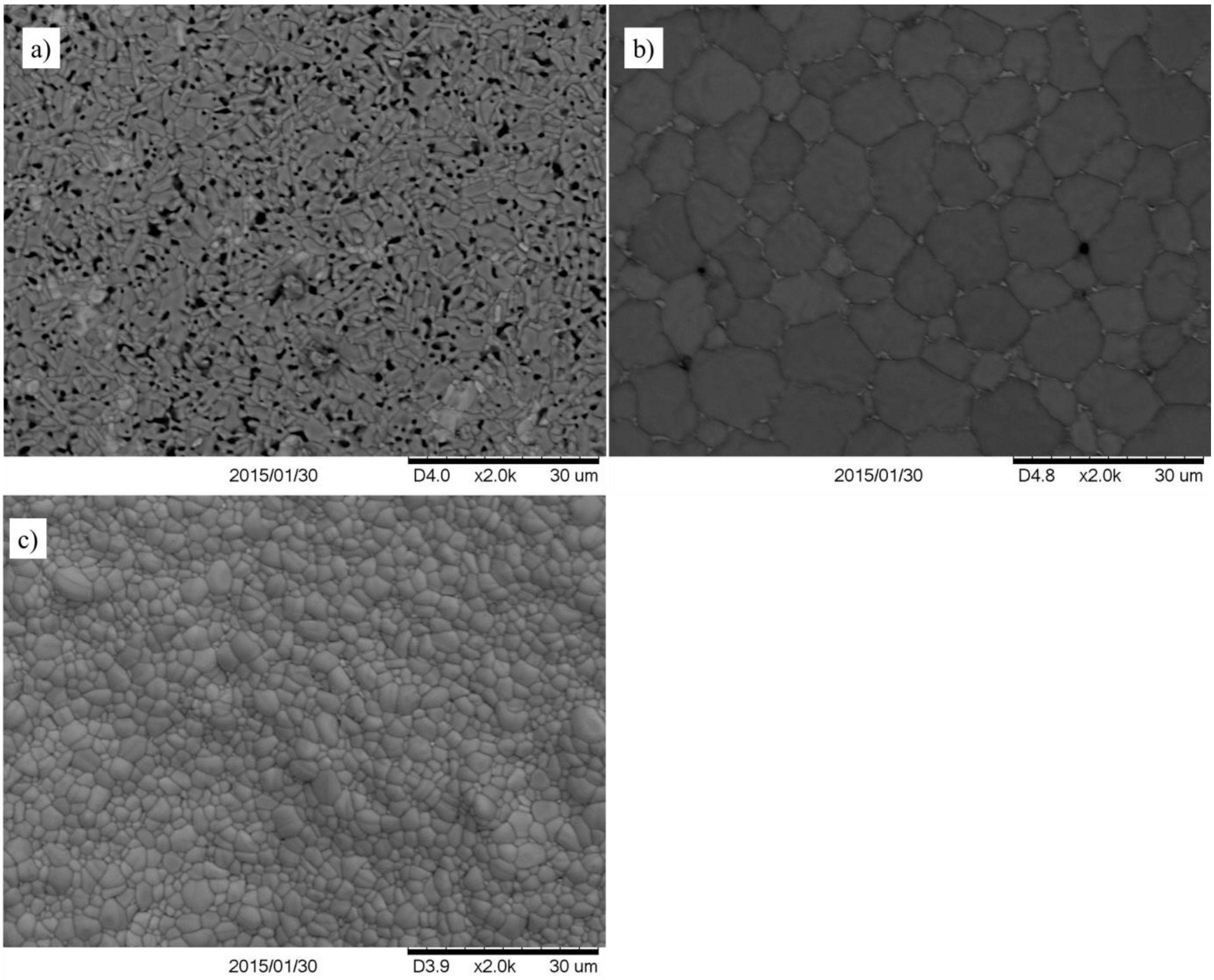

Figure S4: SEM images of as-prepared a) YBCO-pellet, b) LBCO-pellet and c) PBCO-pellet, all with a magnification of 2000x.

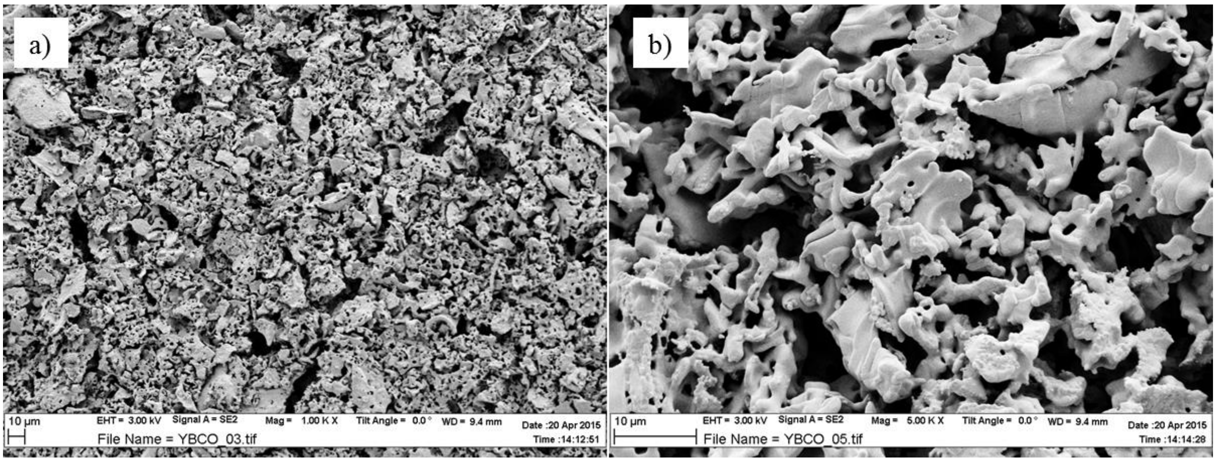

Figure S5: SEM images of an as-prepared YBCO granule at a magnification of a) 1000x and b) 5000x.

c. BET

The specific surface area determined for the produced YBCO granules is 0.25 ± 0.012 m^2 g^{-1}.

d. TGA data

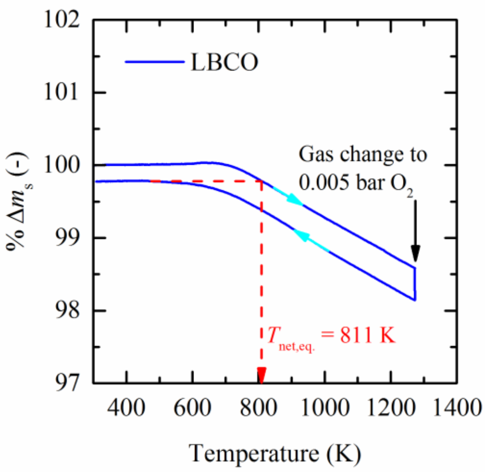

Figure S6: Percent weight change vs. temperature showing exemplary the derivation of $T_{\mathrm{net,eq}}$ of LBCO.

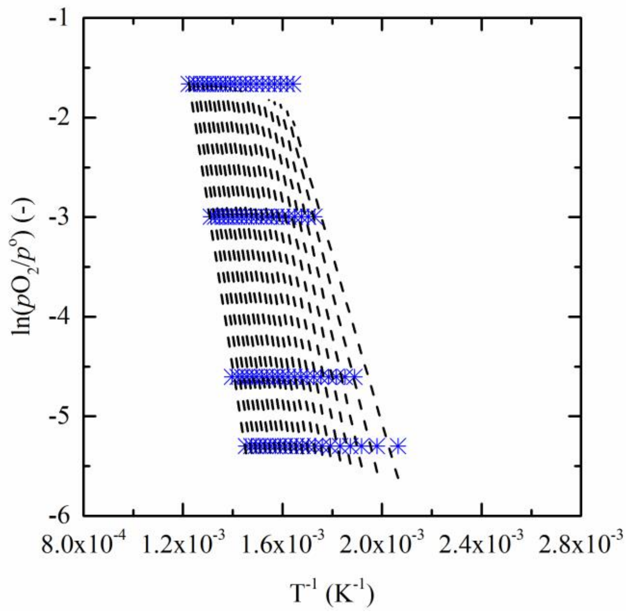

Figure S7: -ln(pO_2/p^o) as a function of T^{-1} of YBCO for δ = 0.0401-0.1400.

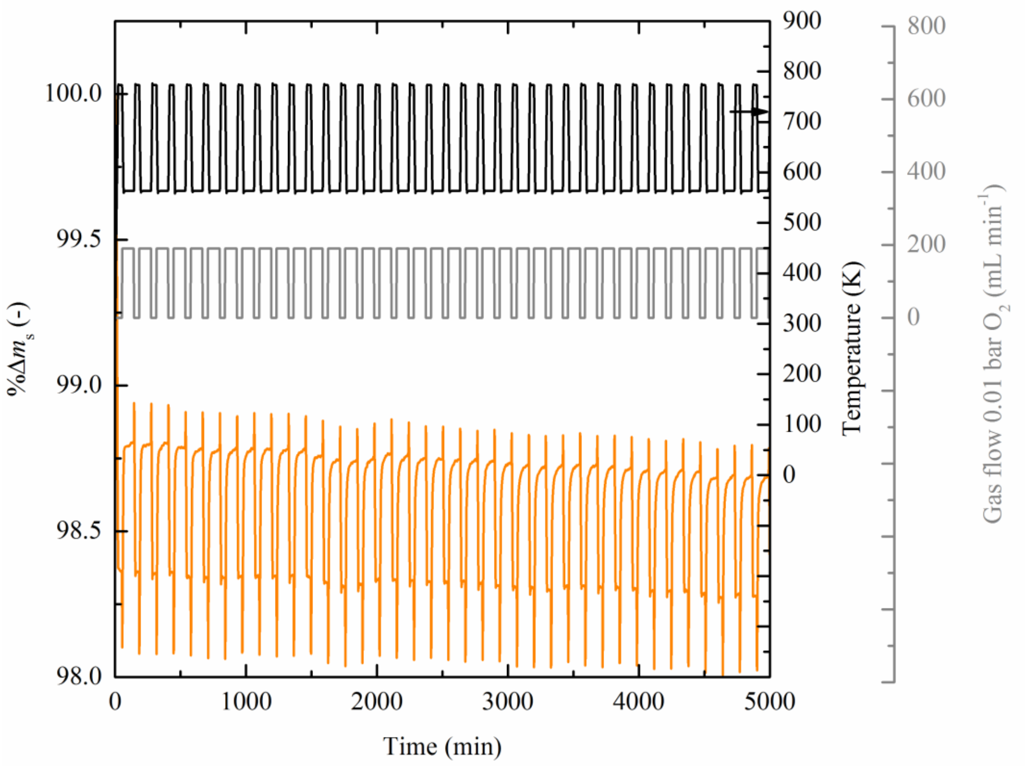

Figure S8: Percent weight change vs. time at 563 and 0.01 bar O_2 during oxidation and 773 K and 0.2 bar O_2 during reduction of YBCO.

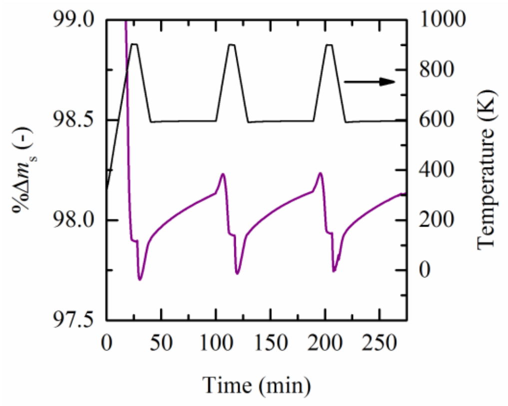

Figure S9: Percent weight change vs. time at 600 K and 0.01 bar O_2 during oxidation and 900 K and 0.2 bar O_2 during reduction of $SrCoO_{3-\delta}$.

e. Molar heat capacity

The molar heat capacity at constant pressure p is defined as

$$c_p = \left(\frac{\partial h}{\partial T} \right)_p \tag{5}$$

where h is the molar enthalpy and T is the temperature.[11] The c_p measurement of YBCO, shown with Fig. S10, was described using Eq. 6 ($R^2 = 0.988$), according to Pankratz *et al.*[12], Satoh *et al.*[13] and Matsuda *et al.*[14], who all measured the molar heat capacities of metal oxides.

$$c_p = 78.75 + 96.49 \cdot 10^{-3} \cdot T - 5.63 \cdot 10^{6} \cdot T^{-2} \tag{6}$$

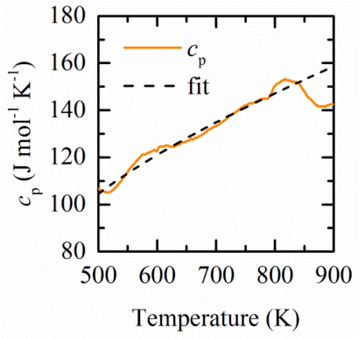

Figure S10: Molar heat capacity, c_p, of YBCO as a function of temperature between 500 and 900 K. The orange line shows the measured data, while the dashed black line shows the result of the least squares fitting ($R^2 = 0.988$).

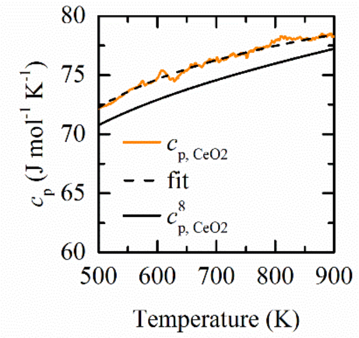

Figure S11: c_p of CeO_2 as a function of temperature between 500 and 900 K. The orange line shows the measured data, while the dashed black line shows the result of the least squares fitting ($R^2 = 0.998$). The solid black line represents the fitting curve of CeO_2 conducted by Pankratz *et al.*[12], revealing on average a deviation to the dashed black line of only 1.94%.

f. PBR data

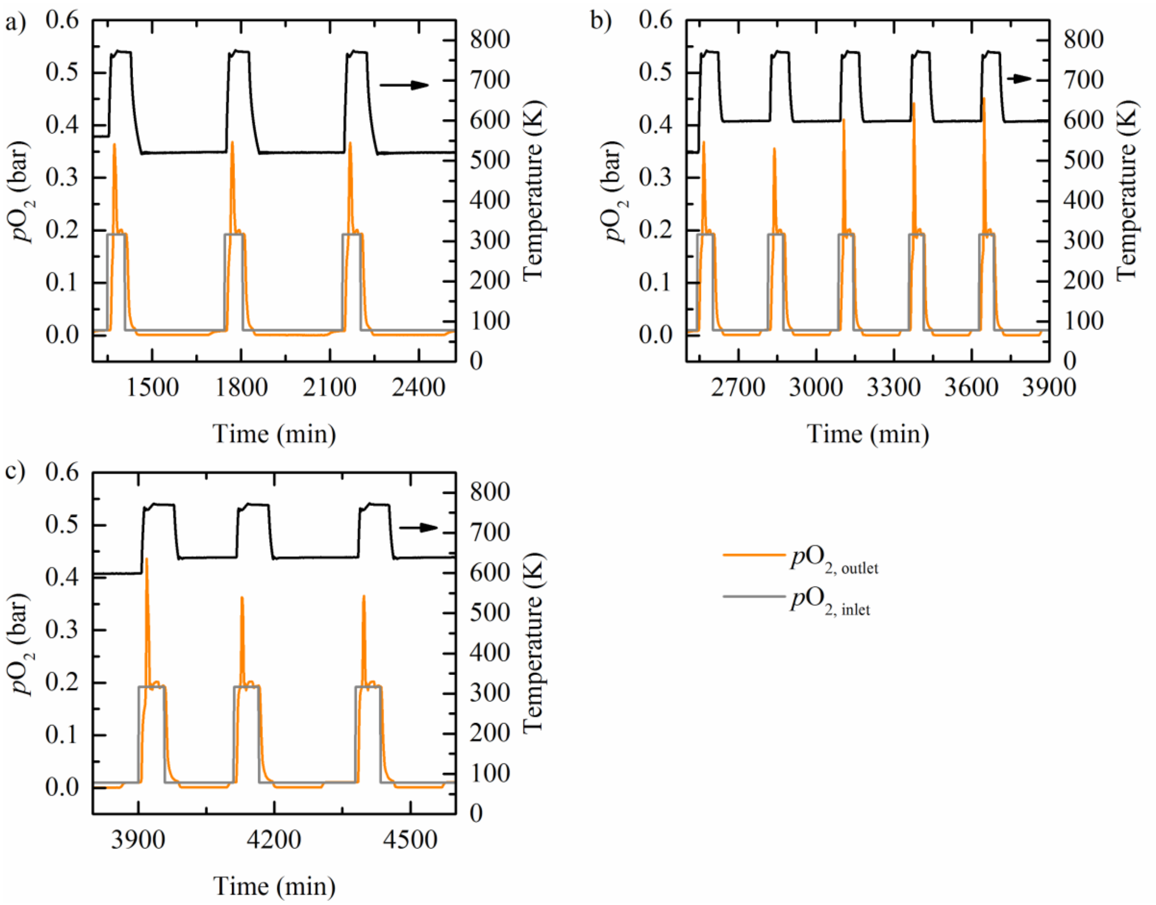

Figure S12: PBR experiments with YBCO for TOS showing pO_2 at the outlet (orange) and inlet (grey) of the packed bed reactor at 773 K and 0.2 bar O_2 during reduction and at 0.01 bar O_2 and a) 523 K, b) 603 K and c) 643 K during oxidation.

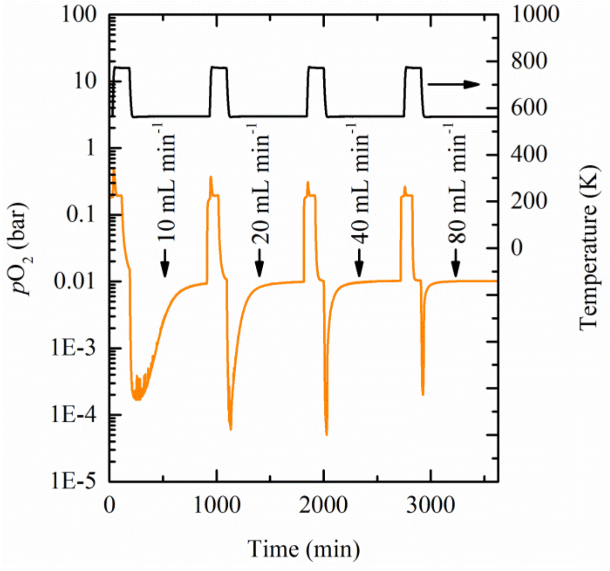

Figure S13: PBR experiment for TOS showing pO_2 at the outlet of the packed bed reactor (orange) vs. time using YBCO granule at 563 K and 0.01 bar O_2 for oxidation and 773 K and 0.2 bar O_2 for reduction. Oxidation cycles 1, 2, 3 and 4 were performed using 10, 20, 40 and 80 mL min^{-1}, respectively.

g. Energy balance equations

Eqs. 7-14 show how the different components of the energy balances of TOS and TOP are calculated.

$$\Delta h_{\mathrm{ha}} = n_{\mathrm{air}} \cdot c_{\mathrm{p,air}} \cdot \Delta T \tag{7}$$

$$\Delta h_{\mathrm{ca}} = (n_{\mathrm{air}} \cdot c_{\mathrm{p,air}} + n_{\mathrm{O_2}} \cdot c_{\mathrm{p,O_2}}) \cdot \Delta T \tag{8}$$

$$\Delta h_{\mathrm{hg}} = (n_{\mathrm{ar}} \cdot c_{\mathrm{p,ar}} + n_{\mathrm{O_2}} \cdot c_{\mathrm{p,O_2}}) \cdot \Delta T \tag{9}$$

$$\Delta h_{\mathrm{cg}} = n_{\mathrm{ar}} \cdot c_{\mathrm{p,ar}} \cdot \Delta T \tag{10}$$

$$\Delta h_{\mathrm{red}} = \frac{\int_{\delta_{\mathrm{i}}}^{\delta_{\mathrm{f}}} \Delta \bar{h}^{\circ}_{\mathrm{O_2}}(\delta)}{\delta_{\mathrm{f}} - \delta_{\mathrm{i}}} \mathrm{d}\delta \tag{11}$$

$$\Delta h_{\mathrm{ox}} = -\Delta h_{\mathrm{red}} \tag{12}$$

$$\Delta h_{\mathrm{hs}} = n_{\mathrm{YBCO}} \cdot c_{\mathrm{p,YBCO}} \cdot \Delta T \tag{13}$$

$$\Delta h_{\mathrm{cs}} = -n_{\mathrm{YBCO}} \cdot c_{\mathrm{p,YBCO}} \cdot \Delta T \tag{14}$$

h. Thermochemical equilibrium analysis

Table S1: Enthalpies of reduction at 298 K ($\Delta \bar{h}^{o*}_{O_2}$) and Gibbs free energies of the oxide reduction at 773 K and 0.2 bar O_2 ($\Delta \bar{g}^{o*}_{O_2}$) and oxide oxidation at 563 K and 0.01 bar O_2 ($-\Delta \bar{g}^{o*}_{O_2}$) of 32 solid metal oxide and six metal/metal oxide pairs at 1 bar, calculated from experiment-derived tabulated thermochemical data.[15]

Product of the oxide oxidation	**Reactant of the oxide oxidation**	$\Delta \bar{h}^{o*}_{O_2}$ **(kJ mol$^{-1}_{O_2}$)**	$\Delta \bar{g}^{o*}_{O_2}$ (kJ mol$^{-1}_{O_2}$)	-$\Delta \bar{g}^{o*}_{O_2}$ (kJ mol$^{-1}_{O_2}$)
Ag	Ag_2O	62.200	-69.258	37.670
Au	Au_2O_3	-53.835	-155.857	122.180
BaO	BaO_2	161.502	30.586	-50.999
Ce_2O_3	CeO_2	762.326	548.879	-594.433
CoO	Co_3O_4	392.376	137.377	-197.789
Cu	Cu_2O	341.414	214.406	-234.032
Cu_2O	CuO	237.773	107.388	-138.780
FeO	$Fe_{0.947}O$	351.621	200.617	-225.642
FeO	Fe_3O_4	604.502	384.080	-427.092
Fe_3O_4	Fe_2O_3	471.956	252.252	-299.649
MnO	Mn_3O_4	464.272	258.260	-300.160
Mn_3O_4	Mn_2O_3	202.816	66.904	-89.115
MoO_2	MoO_3	312.294	194.360	-211.498
Na_2O	Na_2O_2	190.454	55.601	-76.819
NbO	NbO_2	750.610	597.440	-623.860
NbO_2	Nb_2O_5	619.232	495.216	-514.498
OsO_2	OsO_4	42.229	57.767	-39.843
PbO	Pb_3O_4	103.923	-14.802	-5.156
Pb_3O_4	PbO_2	54.907	-61.592	30.437
Rh_2O	RhO	120.729	-0.946	-30.394
RhO	Rh_2O_3	345.017	206.184	-246.407
Ru	RuO_2	305.014	163.159	-186.445
Sb_2O_3	SbO_2	338.086	200.645	-238.726
SnO	SnO_2	590.106	416.749	-448.407
TiO	Ti_2O_3	871.108	721.944	-744.989
Ti_2O_3	Ti_3O_5	711.280	610.297	-615.919
Ti_3O_5	Ti_4O_7	753.958	629.671	-676.400
Ti_4O_7	TiO_2	748.934	581.439	-613.943

Tl_2O	Tl_2O_3	185.400	60.261	-89.005
VO	V_2O_3	710.442	574.038	-596.414
V_2O_3	V_2O_4	416.726	280.121	-297.735
V_2O_4	V_2O_5	246.856	97.848	-128.720
WO_2	$WO_{2.72}$	531.833	403.787	-423.569
$WO_{2.72}$	$WO_{2.9}$	432.344	308.756	-327.262
$WO_{2.9}$	$WO_{2.96}$	496.500	369.029	-388.529
$WO_{2.96}$	WO_3	397.500	264.730	-288.098
Zn	ZnO	700.920	534.972	-566.650
Zr	ZrO_2	1097.463	939.385	-967.471

i. Electronic structure calculations

Table S2: DFT-calculated free energies of forming oxygen vacancies at 298 K ($\Delta G_V[O]$), enthalpies of the oxide reduction at 298 K ($\Delta\bar{h}^{o*}_{O_2}$) and Gibbs free energies of oxide reduction at 773K and 0.2 bar O_2 ($\Delta\bar{g}^{o*}_{O_2}$) and oxidation at 563K and 0.01 bar O_2 ($-\Delta\bar{g}^{o*}_{O_2}$) for $LaCoO_3$-LBCO(010), $BaCoO_3$-LBCO(010), $PrCoO_3$-PBCO(010), $BaCoO_3$-PBCO(010), $YCoO_3$-YBCO(010) and $BaCoO_3$-YBCO(010) perovskite facets. All data is at 1 bar.

Perovskites	**ΔG_V[O] (eV)**	$\Delta\bar{h}^{o*}_{O_2}$ **(** kJ $mol^{-1}_{O_2}$ **)**	$\Delta\bar{g}^{o*}_{O_2}$ **(** kJ $mol^{-1}_{O_2}$ **)**	$-\Delta\bar{g}^{o*}_{O_2}$ **(** kJ $mol^{-1}_{O_2}$ **)**
$LaCoO_3$-LBCO(010)	0.15	215.44	86.80	-112.69
$BaCoO_3$-LBCO(010)	0.53	299.97	165.72	-192.35
$PrCoO_3$-PBCO(010)	-0.21	134.01	10.77	-35.95
$BaCoO_3$-PBCO(010)	0.54	302.95	168.51	-195.16
$YCoO_3$-YBCO(010)	-0.59	49.43	-68.21	43.76
$BaCoO_3$-YBCO(010)	0.93	389.19	249.03	-276.43

3. Nomenclature

ca	cooling air
cg	cooling gas
cs	cooling solid
$c_{p,\,air}$	molar heat capacity of air (J mol^{-1} K^{-1})
$c_{p,\,O2}$	molar heat capacity of air (J mol^{-1} K^{-1})
$c_{p,\,YBCO}$	molar heat capacity of YBCO (J mol^{-1} K^{-1})
ha	heating air
hg	heating gas
hs	heating solid
n_{air}	mole number of air (mol)
n_{O2}	mole number of oxygen (mol)
n_{YBCO}	mole number of YBCO needed to sequestrate 1 mol O_2 (mol)
ΔT	Difference between oxidation and reduction temperatures (K)

4. References

1. A. J. Medford, A. Vojvodic, F. Studt, F. Abild-Pedersen and J. K. Nørskov, *J. Catal.*, 2012, **290**, 108-117.
2. R. Michalsky, Y. J. Zhang, A. J. Medford and A. A. Peterson, *J. Phys. Chem. C*, 2014, **118**, 13026-13034.
3. H. Koster and F. H. B. Mertins, *Powder Diffr.*, 2003, **18**, 56-59.
4. B. Roy and S. Das, *J. Alloys Compd.*, 2011, **509**, 5537-5544.
5. Z. H. Zeng, F. Calle-Vallejo, M. B. Mogensen and J. Rossmeisl, *PCCP*, 2013, **15**, 7526-7533.
6. R. Michalsky, V. Botu, C. M. Hargus, A. A. Peterson and A. Steinfeld, *Adv. Energy Mater.*, 2014, **4**, 1401082.
7. T. Nakajima, M. Ichihara and Y. Ueda, *J. Phys. Soc. Jpn.*, 2005, **74**, 1572-1577.
8. M. M. Seikh, V. Pralong, O. I. Lebedev, V. Caignaert and B. Raveau, *J. Appl. Phys.*, 2013, **114**.

9. T. Vogt, P. M. Woodward, P. Karen, B. A. Hunter, P. Henning and A. R. Moodenbaugh, *Phys. Rev. Lett.*, 2000, **84**, 2969-2972.
10. W. Zhou, C. T. Lin and W. Y. Liang, *Adv. Mater.*, 1993, **5**, 735-738.
11. M. J. Moran, H. N. Shapiro, D. D. Boettner and M. B. Bailey, *Fundamentals of Engineering Thermodynamics, 7th edition*, USA, 2011.
12. L. B. Pankratz, *Thermodynamic Properties of Elements and Oxides*, USA, 1982.
13. H. Satoh, M. Takagi, K. Kinukawa and N. Kamegashira, *Thermochim. Acta*, 1997, **299**, 123-126.
14. T. Matsuda, S. Yamanaka, K. Kurosaki, M. Uno and S. Kobayashi, *J. Alloys Compd.*, 2001, **322**, 77-81.
15. I. Barin, *Thermochemical Data of Pure Substances*, 1993.